BEAM HEAT LOAD ANALYSIS WITH COLDDIAG: A COLD VACUUM CHAMBER FOR DIAGNOSTICS

R. Voutta *, S. Casalbuoni, S. Gerstl, A. W. Grau, T. Holubek, D. Saez de Jauregui, Karlsruhe Institute of Technology (KIT), Karlsruhe, Germany
R. Bartolini, M. P. Cox, E. C. Longhi, G. Rehm, J. C. Schouten, R. P. Walker, Diamond Light Source, Oxfordshire, England
M. Migliorati, B. Spataro, INFN/LNF, Frascati, Italy

Abstract

The knowledge of the heat intake from the electron beam is essential to design the cryogenic layout of superconducting insertion devices. With the aim of measuring the beam heat load to a cold bore and understanding the responsible mechanisms, a cold vacuum chamber for diagnostics (COLDDIAG) has been built. The instrumentation comprises temperature sensors, pressure gauges, mass spectrometers and retarding field analyzers, which allow to study the beam heat load and the influence of the cryosorbed gas layer. COLDDIAG was installed in the storage ring of the Diamond Light Source from September 2012 to August 2013. During this time measurements were performed for a wide range of machine conditions, employing the various measuring capabilities of the device. Here we report on the analysis of the measured beam heat load, pressure and gas content, as well as the low energy charged particle flux and spectrum as a function of the electron beam parameters.

INTRODUCTION

Superconducting insertion devices (IDs) can generate higher magnetic fields than permanent magnet IDs with the same gap and period length, increasing the photon flux and the brilliance. The cryogenic design of superconducting IDs requires the knowledge of the beam heat load to the cold vacuum chamber. Potential beam heat load sources are synchrotron radiation, geometric and resistive wall impedance, and electron and/or ion bombardment. To understand the discrepancies between the calculated predictions and the beam heat load observed in several devices [1–3], a cold vacuum chamber for beam heat load diagnostics (COLDDIAG) has been built [4]. After its installation in the Diamond Light Source (DLS) storage ring in September 2012, the beam heat load, pressure and gas content, and the low energy charged particle flux and spectrum have been measured during user operation and in dedicated machine physics sessions until August 2013. A subsequent offline calibration of the beam heat load measurements [5] has been performed in order to remove the contribution of the thermal transitions to the beam heat load from the measurements, which turned out to be about half of the total measured heat load. In the following we present some of the main results from the beam heat load analysis of the data taken with COLDDIAG at the DLS.

* robert.voutta@kit.edu

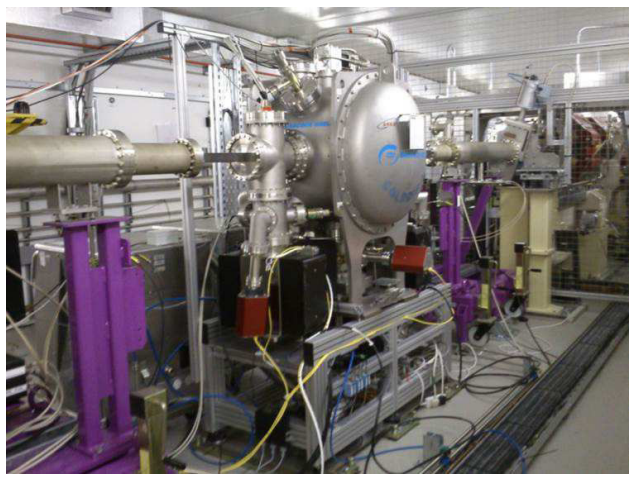

Figure 1: COLDDIAG installed in the DLS storage ring.

EXPERIMENTAL SETUP

COLDDIAG is composed of three sections, an upstream and downstream warm section and a cold section in between. The cold section is cooled down by a Sumitomo RDK-415D cryocooler to a base temperature of about 4 K. Each section is equipped with a diagnostic port, providing a retarding field analyser (RFA), a residual gas analyser (RGA) and a pressure gauge. Eight temperature sensors in each warm section and 24 temperature sensors in the cold section allow to record the temperature distribution along the beam tube (liner) and in the cold UHV chamber. The beam heat load is calibrated using 6 heaters attached to the liner, one in each warm section and four in the cold section. The heaters in the cold section can also be used to regulate the temperature of the cold liner to a specific temperature (usually 20 K) during operation. Two additional heaters, one at each thermal transition to the cold liner, were installed after the removal from the DLS in order to reproduce the temperatures at the thermal transitions during the measurements in an offline calibration. Figure 1 shows COLDDIAG installed in a straight section of the DLS storage ring.

BEAM HEAT LOAD

The beam heat load was measured during user operation and in various machine physics sessions, scanning a wide range of machine parameters. The measurements discussed here were performed with the liner at a fixed temperature

ISBN 978-3-95450-168-7

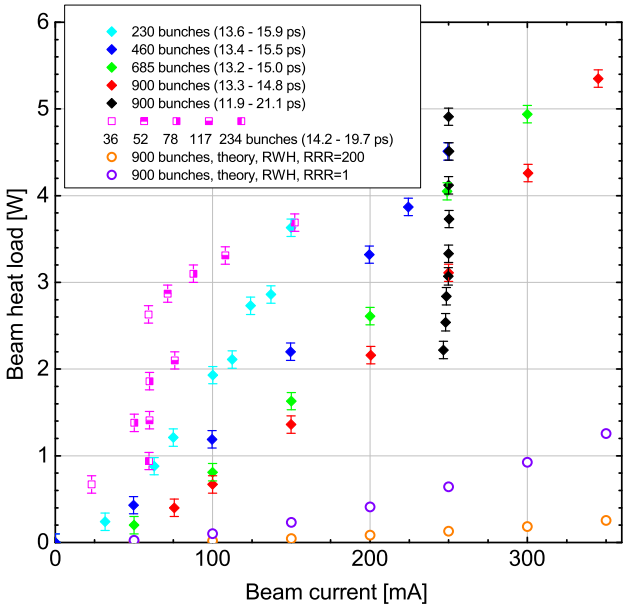

Figure 2: Beam heat load measured for different filling patterns and the cold beam tube at 20 K. The error is estimated to be 0.1 W.

(20 K), resulting in a greater accuracy compared to measurements with a variable liner temperature, because the heat load can be read directly as a difference in heating power. Figure 2 shows the measured beam heat load as a function of beam current for the covered range of bunch lengths, bunch currents and bunch spacings.

It can be readily seen that for the same beam current the beam heat load increases with a decreasing number of bunches (i.e. higher bunch charge). For beam current ramps (step-wise increase of beam current for a fixed filling pattern) the bunch length rises with beam current, but in a realtively small range (10% - 20%). The black points represent the beam heat load measured by increasing the bunch length by ≈ 77% with a fixed filling pattern (250 mA, 900 bunches).

These beam heat load data are plotted as a function of the bunch length in Fig. 3, with several models for heating due to RF effects applied to them, namely an empirical power law ($P \propto \sigma^{-1.4}$), resistive wall heating in the normal ($P \propto \sigma^{-3/2}$) and anomalous ($P \propto \sigma^{-5/3}$) regime [6], step transitions ($P \propto \sigma^{-1}$) [7] and a combination of step transitions and resistive wall heating. The anomalous skin effect and the step transitions do not fit to the measured data, while the normal skin effect is just within the errors. The other two models provide one additional fit parameter and represent the data very well.

Simulations of heating due to geometric and resistive wall impedances on the COLDDIAG geometry [7] did not indicate a significant contribution. Figure 2 shows the calculated values of resistive wall heating for cold high purity copper ($RRR = 200$, anomalous skin effect) and for low purity copper ($RRR = 1$, normal skin effect), considering the same bunch length as for the beam current ramps

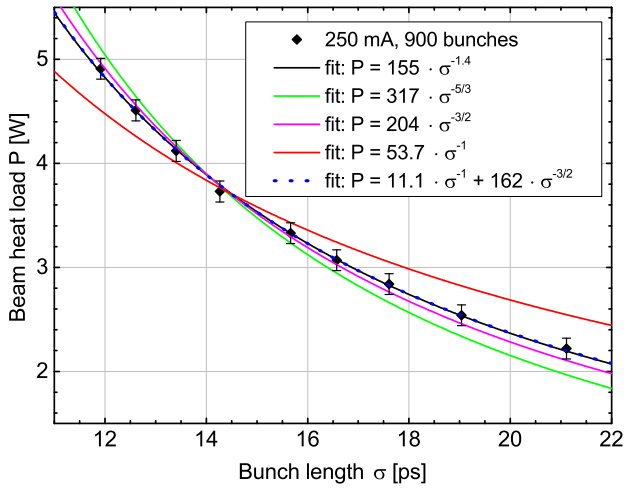

Figure 3: Bunch length dependence of the beam heat load compared with different models.

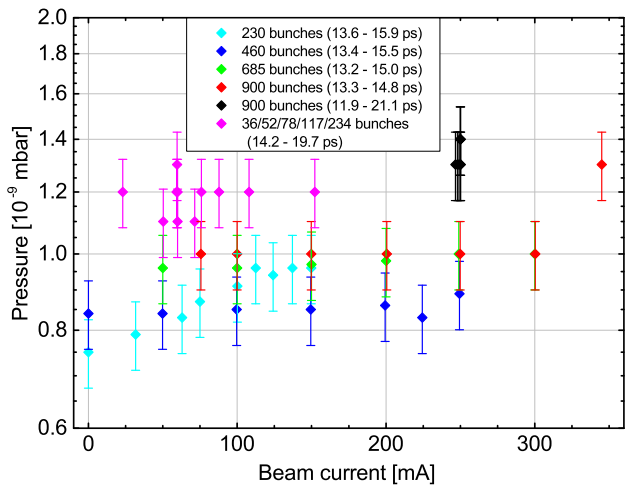

Figure 4: Pressure measured for different filling patterns and the cold beam tube at 20 K. The estimated error is 10%.

PRESSURE AND GAS CONTENT

The total pressure has been measured in the three sections of COLDDIAG and in the upstream and downstream pumping station. Since the upstream pressure gauge is located before the absorber that protects the COLDDIAG liner, it shows a linear pressure increase due to synchrotron radiation hitting the beam pipe.

In the cold section, where the temperature is kept at 20 K, no significant pressure change is visible (see Fig. 4). The difference in pressure between the measurements seems to be due to different thermal outgassing, which depends on the history.

The gas composition has been measured with the RGAs in each diagnostic port up to an atomic mass of 100 u. In Fig. 5 a typical mass spectrum in the cold section is shown. It features the main contributions at 2 u, 18 u and 28 u for

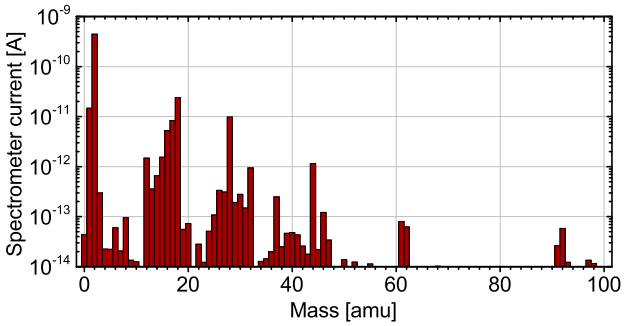

Figure 5: Typical mass spectrum of the residual gas in the COLDDIAG cold section.

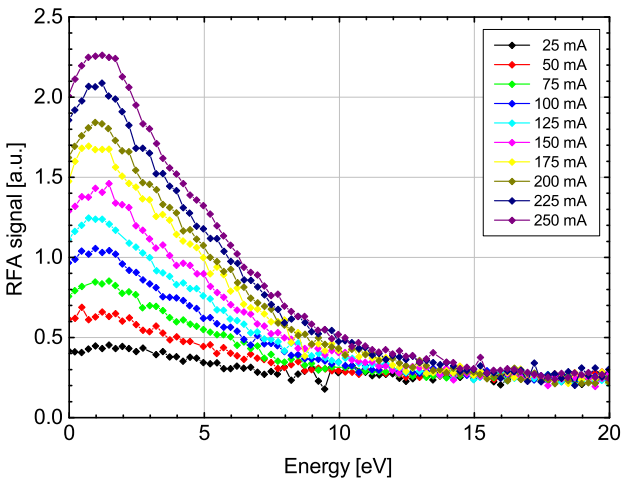

Figure 6: Energy spectrum of low energy electrons during a beam current ramp, measured with the RFA placed in the cold section.

H, H_2O and CO respectively, characteristic for an unbaked system. In accordance with the total pressure the spectrum does not change significantly with beam current.

However, this does not exclude heating originated from the interaction of the beam with the cryosorbed gas layer, since the base pressure is relatively high and the effect could be shadowed by the background pressure due to thermal outgassing.

LOW ENERGY ELECTRONS

The spectrum of low energy charged particles hitting the liner has been measured with the RFAs up to 250 eV. For positively charged particles, i.e. with a negative voltage applied to the collector of the RFA, no significant contribution was found. When a positive voltage is applied to the collector the particles can be identified as electrons and their energy spectrum exhibits a peak at 1 eV, which converges to the base line by 20 eV.

Figure 6 shows this part of the spectrum in the cold section for a beam current ramp in 25 mA steps. From the peak values it can already be anticipated that the total flux of low energy electrons increases linearly with beam current. Figure 7 demonstrates this fact for three different beam current ramps in all three sections of COLDDIAG.

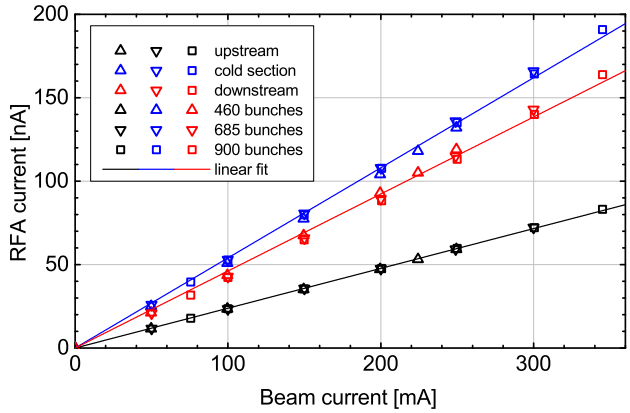

Figure 7: Total flux of low energy electrons hitting the beam chamber wall in the three sections of COLDDIAG for three different beam current ramps.

The linear increase is typical for photoelectrons, which can be created by reflected synchrotron radiation. This is in agreement with the fact that the flux is higher downstream than upstream, because of the greater distance to the absorber. In the cold section the cryosorbed gas layer acts as an additional source of low energy electrons, resulting in the highest flux. However, electron bombardment cannot explain the measured beam heat load, since even a conservative estimate of the deposited power is below 1 mW. But it is possible that the low energy electrons responsible for heating the liner, do not hit the walls where the slots to the RFA are and/or that the RFA itself prevents electron build-up at its position by absorbing the primary electrons.

CONCLUSION

Extensive beam heat load measurements were performed with COLDDIAG at the Diamond Light Source. The measured beam heat load is at 300 mA about 5 times (RRR = 1) to 20 times (RRR = 200) higher than predicted from theory. Direct synchrotron radiation can be excluded as a possible heat source. Heating due to electron and/or ion bombardment could not be verified.

REFERENCES

[1] E. Wallén, G. LeBlanc, Cryogenics 44, 879 (2004).

[2] S. Casalbuoni et al., Phys. Rev. ST Accel. Beams 10, 093202 (2007).

[3] J.C. Schouten, E.C.M. Rial, THPC179, IPAC'11, San Sebastián, Spain (2011).

[4] S. Gerstl et al., THPC159, IPAC'11, San Sebastián, Spain (2011).

[5] S. Gerstl et al., Phys. Rev. ST Accel. Beams 17, 103201 (2014).

[6] W. Chou, F. Ruggiero, CERN LHC Project Note 2 (SL/AP), 1995.

[7] S. Casalbuoni et al., JINST 7, P11008 (2012).

ISBN 978-3-95450-168-7